ATOMIC LAYER DEPOSITION

INTERNATIONAL JOURNAL

OPEN ACCESS **Research Article**

Atmospheric-pressure plasma-enhanced spatial atomic layer deposition of silicon nitride at low temperature

Jie Shen[1], Fred Roozeboom[2], Alfredo Mameli[1]

1   *TNO / Holst Centre, High Tech Campus 31, 5656 AE, Eindhoven, Netherlands*
2   *Faculty of Science & Technology, University of Twente, 7500 AE Enschede, Netherlands*
Corresponding author: Alfredo Mameli (alfredo.mameli@tno.nl)

Abstract

Atmospheric-pressure plasma-enhanced spatial atomic layer deposition (PE-spatial-ALD) of SiN_x is demonstrated for the first time. Using bis(diethylamino)silane (BDEAS) and N_2 plasma from a dielectric barrier discharge source, a process was developed at low deposition temperatures (≤ 250 °C). The effect of N_2 plasma exposure time and overall cycle time on layer composition was investigated. In particular, the oxygen content was found to decrease with decreasing both above-mentioned parameters. As measured by depth profile X-ray photoelectron spectroscopy, 4.7 at.% was the lowest oxygen content obtained, whilst 13.7 at.% carbon was still present at a deposition temperature of 200 °C. At the same time, deposition rates up to 1.5 nm/min were obtained, approaching those of plasma enhanced chemical vapor deposition and thus opening new opportunities for high-throughput atomic-level processing of nitride materials.

Key words: Spatial ALD, silicon nitride (SiN_x), spatial atomic layer deposition, atmospheric pressure, low temperature (250 °C)

1. Introduction

Silicon nitride is an essential material in device fabrication, with applications ranging from microelectronics, thin-film transistors, optoelectronics, encapsulation and patterning [1–3]. For many of these applications SiN_x should be deposited at relatively low temperatures (< 350 °C) with excellent material properties and uniformity over large areas as well as 3D topographies.

Atomic layer deposition (ALD) and in particular plasma-enhanced ALD (PE-ALD) can fulfil all of the above listed requirements. In conventional, temporal ALD, a substrate is cyclically exposed to a precursor and a co-reactant that are separated in time and undergo self-limiting surface reactions, thus allowing for Ångström-level thickness control and unparalleled uniformity and conformality over 3D substrates. In the case of PE-ALD, the plasma-activated co-reactant can effectively reduce the thermal budget required for film deposition, and often allows for improved layer properties, compared to those of layers grown with thermal ALD [4, 5].

Hence, extensive research has been devoted to PE-ALD of SiN_x using different types of precursors, plasma-feed gases and types of plasmas [2, 3, 6–10]. Nevertheless, high-quality PE-ALD of SiN processes often suffer from low deposition rates which can ultimately hamper industrial applicability. As a result, plasma-enhanced chemical vapor deposition (PE-CVD) is often favored by industry because of its high deposition rate (3−5 nm/min), unless features with challenging aspect ratios need to be coated. Furthermore, deposition rates of ~50 nm/min and as high as 120 nm/s have been reported using atmospheric-pressure PE-CVD [11, 12].

A way to bridge the gap in deposition rates between PE-CVD and PE-ALD, and thus enable high-throughput ALD, can be achieved by separating precursor and co-reactant in space rather than in time, this method is known as spatial ALD [13]. In spatial mode, the ALD precursor and co-reactant are continuously dosed on a reciprocating or rotating substrate, and no extensive chamber-purge steps are needed to keep the precursor and co-reactant from reacting in the gas-phase (CVD-like reaction). Therefore much shorter ALD cycle times can be achieved [14]. Most of the literature on spatial ALD concerns metal oxides produced either by thermal or plasma-enhanced spatial ALD, [4, 15−17] and only a few examples have been published for spatial-ALD of metallic films (Ag and Cu) [18, 19]. To our knowledge, no attempts have been reported so far to deposit nitrides in an atmospheric-pressure spatial ALD set-up.

In this work we report for the first time on the atmospheric-pressure spatial ALD process of low temperature (≤ 250 ºC) SiN_x using bis(diethylamino)silane (BDEAS) as the silicon precursor and an N_2 plasma as the co-reactant, generated from a direct dielectric barrier discharge (DBD) plasma source. We investigate the saturation behavior of the two half-reactions by spectroscopic ellipsometry and study the influence of plasma exposure time on the incorporation of impurities. Such first round of optimization resulted in oxygen impurities as low as 4.7 at.% and deposition rates up to 1.5 nm/min which are 8 to 42 times faster than those for temporal ALD processes based on similar chemistries. We believe that the results presented in this work can open up possible pathways for high-throughput spatial ALD of high-quality nitrides at atmospheric pressure, thereby expanding the toolbox of high-throughput atomic-level processing.

1. Experimental

2.1. Materials and reactor

All experiments in this work were performed using a custom-built atmospheric pressure spatial ALD rotary reactor, as illustrated in Figure 1. A detailed description of the reactor can be found elsewhere [20, 21]. BDEAS was kept at room temperature in a stainless steel bubbler and dosed using an Ar bubbling flow of 150 sccm with an additional 850 sccm of Ar as dilution, unless differently specified. For the plasma co-reactant, a nitrogen flow of 8000 sccm of N_2 (99.999%) was used as the plasma feeding gas. A home-built atmospheric-pressure DBD plasma source operated at a voltage of 120 V and frequency of 75 kHz was employed [21−23]. SiN_x layers were deposited on Si substrate wafers at deposition temperatures between 150 ºC and 250 °C. Higher deposition temperatures were not explored due to thermal constraints on the currently employed DBD plasma source. In such spatial ALD setup, the substrate is rotated under continuous gas flows of BDEAS and N_2 plasma, which are separated by N_2 gas curtains. Each rotation of the substrate underneath the injector head corresponds to one spatial ALD cycle.

Because of the fixed geometry of the injector and the reactor design, the exposure times of the precursor and of the co-reactant, as well as their purge times, are coupled. The exposure time of the substrate to the precursors/co-reactant, t_{exp}, can be calculated using Equation 1:

$$t_{exp} = \frac{W}{2\pi r f} \tag{1}$$

where W is the width of the deposition zone, r the radial distance from the center of the wafer, and f the rotation frequency in rotations per minute (RPM). The rotation speed was varied between 10 and 80 RPM, corresponding to exposure times ranging from 30 ms to 400 ms.
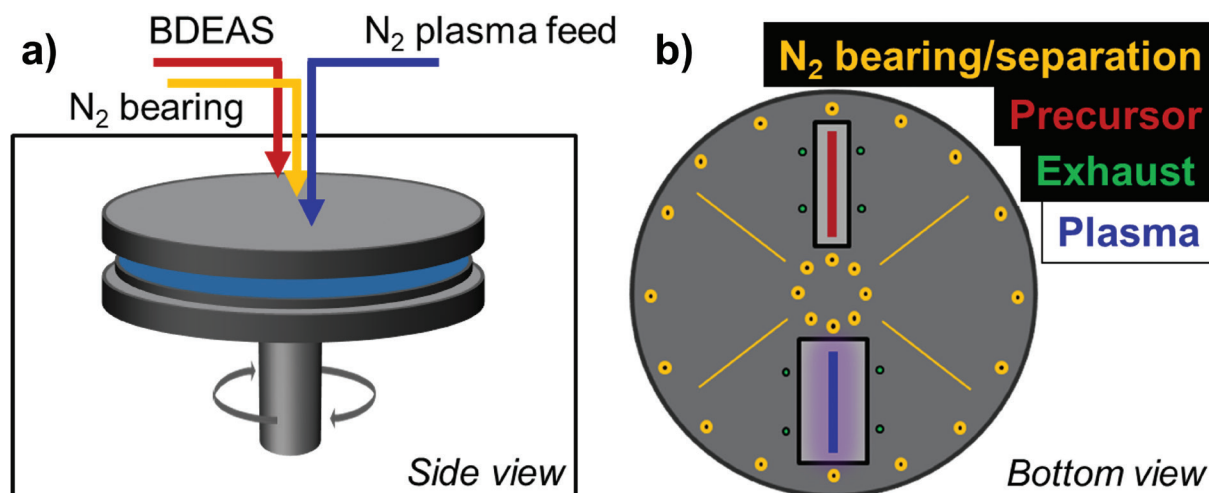
Figure 1. Schematic views of **(a)** the 150-mm wafer lab-scale reactor and **(b)** the bottom-side of the spatial ALD injector head. The N_2 bearing gas streams are controlled in such a way that the substrate is coated at close proximity.

2.2. Decoupling the effect of each half-reaction

As mentioned above, due to the fixed geometry of the reactor all exposure and purge times are coupled and defined by the rotation speed. The total dose (partial pressure times exposure time, $p \cdot t_{exp}$) can be changed in order to be able to decouple the effect of each half-reaction. Hence, for a fixed rotation speed, by varying the partial pressure of the precursor, one can obtain the saturation curve for the precursor half-reaction while keeping the plasma exposure time constant. From the precursor saturation behavior, the total dose required for precursor saturation can be calculated at any given rotation speed. By ensuring precursor saturation while changing the RPM, the effect of the plasma half-reaction exposure time can also be investigated, provided the 'purge times' are long enough to avoid CVD-like reactions.

2.3. Analytical methods

The growth of SiN_x was investigated by depositing on 150-mm double-polished Si (100) wafers. SiN_x film thickness and optical properties were measured by *ex-situ* spectroscopic ellipsometry (SE) using a Horiba UVISEL II. Film thicknesses were extracted using a Tauc-Lorentz model in the spectral range of 1.5–5 eV. The chemical composition and stoichiometry of the SiN_x films were obtained by X-ray photoelectron spectroscopy (XPS), using a Thermo Scientific K-Alpha spectrometer with a monochromatic Al Kα X-ray source. Depth profiles were measured by sputtering with Ar^+ ions using 500 eV, with steps of 15 s. The relative hydrogen content was estimated by Fourier transform infrared spectroscopy (FTIR) of the SiN_x films, using a VERTEX 70 spectrometer from Bruker. Absorbance spectra were collected within the wavenumber range of 650–4000 cm^{-1} with a resolution of 8 cm^{-1} using a room temperature deuterated tri-glycine sulfate (DTGS) detector. The H-concentration from FTIR spectra was evaluated based on the Lanford and Rand method,[24] using the absorption cross-sections, σ, $\sigma_{Si-H} = 7.4 \times 10^{-18}$ cm^2 and $\sigma_{N-H} = 5.3 \times 10^{-18}$ cm^2.

3. Results and discussion

3.1. Process development

Figure 2 shows the SiN_x film thickness as a function of the number of atmospheric pressure-PE-spatial-ALD cycles. A rotation speed of 20 RPM was chosen for this set of experiments to ensure long enough precursor and plasma exposures. This corresponds to exposure times between 109 ms and 200 ms for
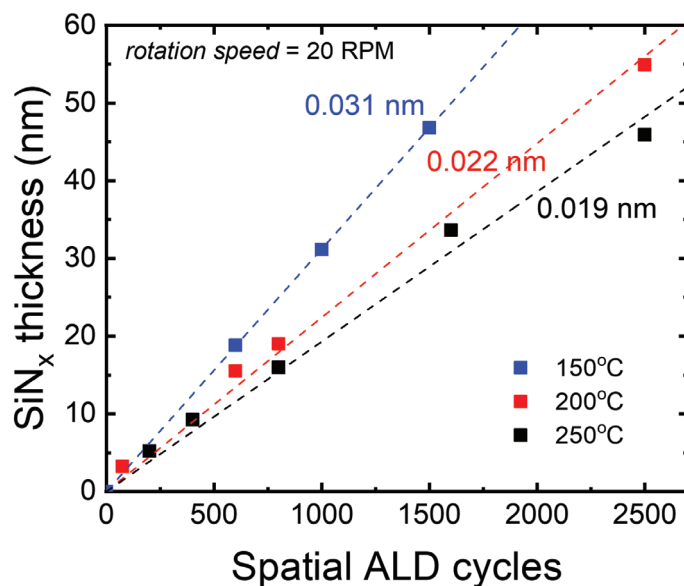
Figure 2. SiN$_x$ layer thickness as a function of the number of spatial ALD cycles, for deposition at 150 °C, 200 °C and 250 °C.

both BDEAS and the N$_2$ plasma and a total ALD cycle time of 3 seconds. A fairly linear thickness increase was observed at all deposition temperatures investigated, from which growth per cycle (GPC) values of 0.31 Å, 0.22 Å and 0.19 Å were obtained for depositions at 150 °C, 200 °C and 250 °C, respectively.

In agreement with earlier literature, the GPC was found to decrease with increasing the deposition temperature, and GPC values were comparable to those reported for low-pressure temporal ALD processes using similar chemistries [8]. These deposition settings, however, resulted in layers with high concentration of O- and C-impurities, tending towards SiO$_x$C$_y$N$_z$ type of materials. In particular, impurity levels as high as 14 at.% O and 13.7 at.% C were measured in the bulk of these films by depth profile XPS. Increasing the deposition temperature from 150 °C to 250 °C led to a decrease in carbon content from 13.7 at.% to 7.5 at.%, and to an opposite trend for O, *i.e.* an increase from 10.3 at.% to 14 at.%.

FTIR was employed to determine the relative hydrogen content in the deposited SiN$_x$ layers. Figure 3a shows an example of an infrared spectrum of a SiN$_x$ layer deposited at 250 °C at 20 RPM. Si-N (~930 cm^{-1}), Si-H (~2190 cm^{-1}), N-H (~3353 cm^{-1}) and NH$_2$ (~1600 cm^{-1}) modes are visible [6]. From these spectra the H-bond densities (Si-H *plus* N-H) were calculated using the method described by Lanford and Rand [24]. As shown in Figure 3b a linear decrease in the number of H-bond density was found upon increasing the deposition temperature from 150 °C to 250 °C, with the lowest value being ~4.7 x 10^{22} cm^{-3}. As a reference typical H-bond densities reported for PE-CVD in the same temperature range are between 6 x 10^{21} (low hydrogen content, <10 at.%)[25] and 2.1 x 10^{22} [24].

3.2. Effect of plasma exposure on the material properties

With the aim of optimizing the deposition process towards high-quality SiN$_x$ we investigated the two separate half-reactions of the spatial ALD process with particular focus on the N$_2$ plasma exposure since it is has been reported that the plasma exposure can have dramatic influence on the impurity levels of SiN$_x$ prepared by PE-ALD [8, 9]. Figures 4a and 4b show the saturation curves for SiN$_x$ grown from BDEAS and N$_2$ plasma at 200 °C and 250 °C. The GPC as a function of the BDEAS partial pressure, *p*, shows saturating behavior for SiN$_x$, indicating self-limiting surface reactions during the precursor step, consistent with ALD behavior and with previous literature on temporal ALD [8, 10]. The rotation speed was kept fixed at 20 RPM to fix the plasma exposure time, while the Ar bubbling flow through the BDEAS precursor was varied from 25 sccm to 150 sccm. For details see the Experimental section. In terms of BDEAS dose, $p \cdot t_{exp}$, sat-
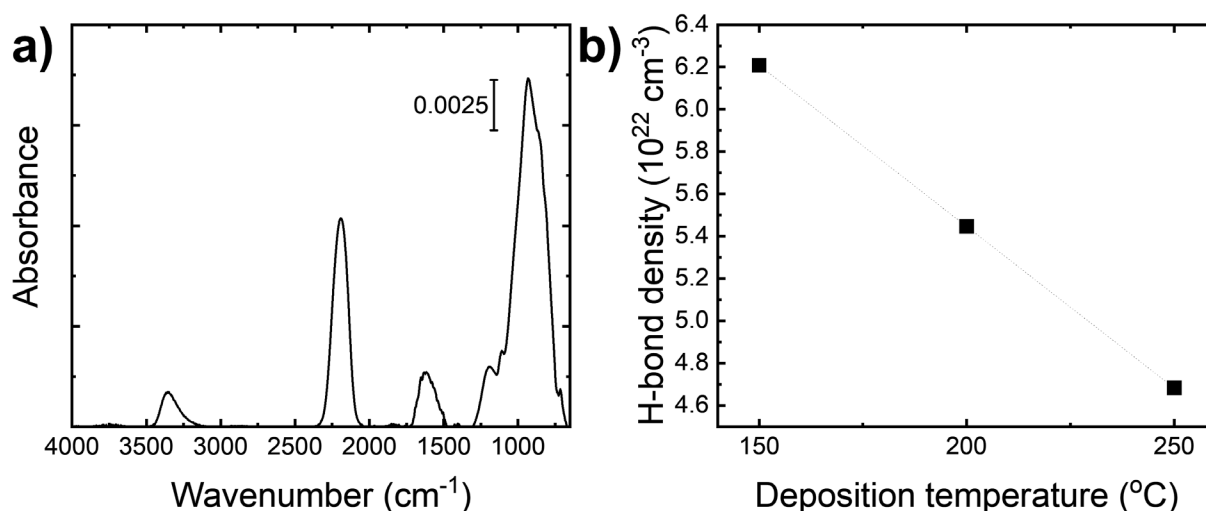
Figure 3. a) Typical infrared spectrum for of a SiN$_x$ layer deposited at 250 °C at 20 RPM, with Si-H and Si-N stretching mode, and N-H stretching and NH$_2$ scissoring mode indicated; **b)** total H-bond density (N-H plus Si-H) derived from FITR measurements.
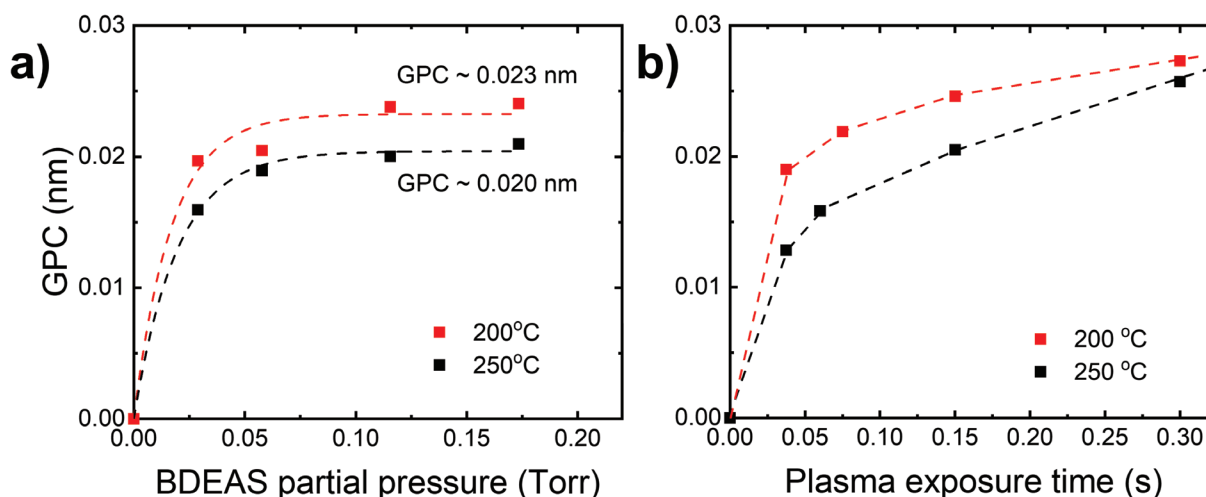

Figure 4. a) shows the growth per cycle (GPC) at (red square) 200 °C and (black square) 250 °C as a function of BDEAS exposure for a fixed N$_2$ plasma exposure time. **b)** GPC at 200 °C (red square) and 250 °C (black square) as a function of the plasma exposure time, for BDEAS exposures above saturation. While the BDEAS exposure results in saturating behavior, the GPC as a function of the plasma exposure time shows a non-ideal behavior.

uration behavior was obtained for precursor doses above 0.015 Torr·s, as shown in Suppl. material 1: fig. S1, which is in good agreement with an earlier report on SiO$_2$ spatial ALD using the same precursor [4].

Conversely, the GPC as a function of the plasma exposure time displays deviation from ideal behavior. A similar effect has been previously observed for temporal PE-ALD of SiN$_x$ using similar precursor chemistries and described as soft-saturating behavior [7, 8]. For example, in the case of bis(tert-butyl)aminosilane, the N$_2$ plasma exposure was observed to directly affect the C-content, through a re-deposition effect,[26] while an Si-H terminated surface upon precursor adsorption was speculated to be responsible for such soft-saturating behavior in the case of di(sec-butyl)aminosilane and neopentasilane as precursors [7].

The refractive index as calculated by optical modelling of the *ex-situ* SE data shows an increasing trend with decreasing N$_2$ plasma exposure time (see Suppl. material 1: table S1 for details), pointing towards denser layers and/or lower impurities (H, C, O). In order to shine light on the effect of N$_2$ plasma exposure observed in our case, XPS depth profiles and FTIR measurements were carried out for different plasma exposures.
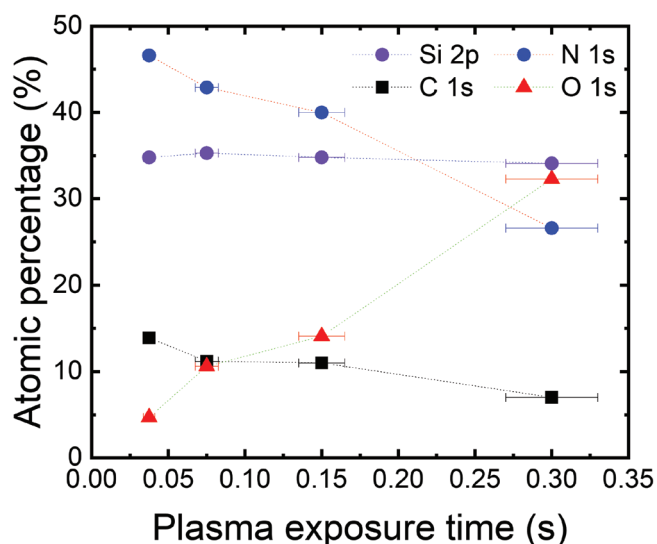
Figure 5. Contents in atomic percentage of O (red triangle), C (black square), Si (purple dot), N (blue dot) in the bulk of the spatial ALD grown SiN$_x$ layers as a function of the N$_2$ plasma exposure time.

Figure 5 shows the SiN$_x$ composition in the bulk of each film as measured by XPS depth profile for different N$_2$ plasma exposure times and at a deposition temperature of 200 °C (see also Suppl. material 1: fig. S2). While the Si at.% remains fairly constant within the measurement error, the O at % shows an almost linear increase with the N$_2$ plasma exposure time and the C at.% decreases slightly with increasing N$_2$ plasma exposure. An optimum thus exists in trying to minimize the C- and the O-content corresponding to a N$_2$ plasma exposure of ~75 ms, *i.e.* a rotation speed of 40 RPM. The lowest O-content was instead obtained for a plasma exposure time of ~37 ms, *i.e.* a rotation speed of 80 RPM. The reasons for such trends are not fully understood at this moment. It can be speculated, however, that a combination of O-impurities present at ppm-levels in the N$_2$ gas and in the background ambient of the reactor are responsible for the incorporation of oxygen, or additionally, that plasma-induced outgassing of the DBD ceramic elements is responsible for O incorporation. Hence, a shorter plasma exposure and an overall shorter cycle time are expected to reduce the oxygen content. On the other hand, longer plasma exposure times might be needed to completely remove the carbonaceous ligands. With this in mind, also a mixture of N$_2$/H$_2$ was tested since H-radicals are known to be effective in removing carbon. However, GPC values as low as 0.06 Å were obtained, similar to earlier reports [8]. Ande *et al.* have used density functional theory to show that such low GPC can be attributed to the formation of an H-terminated surface that is short of suitable adsorption sites for the subsequent precursor step [27].

By optimizing the plasma exposure time to 37 ms, together with an overall ALD cycle time of 750 ms, SiN$_x$ layers with only 4.7 at.% O could be obtained, yet with 13.9 at.% C. Figure 6a shows that the absolute oxygen content drastically decreases within the bulk of the SiN$_x$ layers when going from 10 RPM (red lines), 40 RPM (black lines) to 80 RPM (blue lines). Conversely, the absolute nitrogen and carbon contents increase. Furthermore, a decrease in hydrogen bond density down to 3.5 x 10^{22} cm^{-3} with increasing rotation speed was derived from FTIR measurements, as shown in Figure 6b. Concurrently, the GPC decreased from 0.27 Å at 10 RPM to 0.19 Å at 80 RPM, which corresponds to an increase in deposition rate from 0.27 nm/min to 1.5 nm/min. See Suppl. material 1: table S1 for more details.

3.3. Comparison to PE-ALD and PE-CVD

Table 1 provides an overview of chemistries, deposition temperatures and rates, and resulting material properties such as film refractive index and composition for PE-CVD, atmospheric pressure PE-CVD, low-pressure temporal ALD, and atmospheric-pressure spatial ALD, at deposition temperatures of 200 °C or 250 °C.
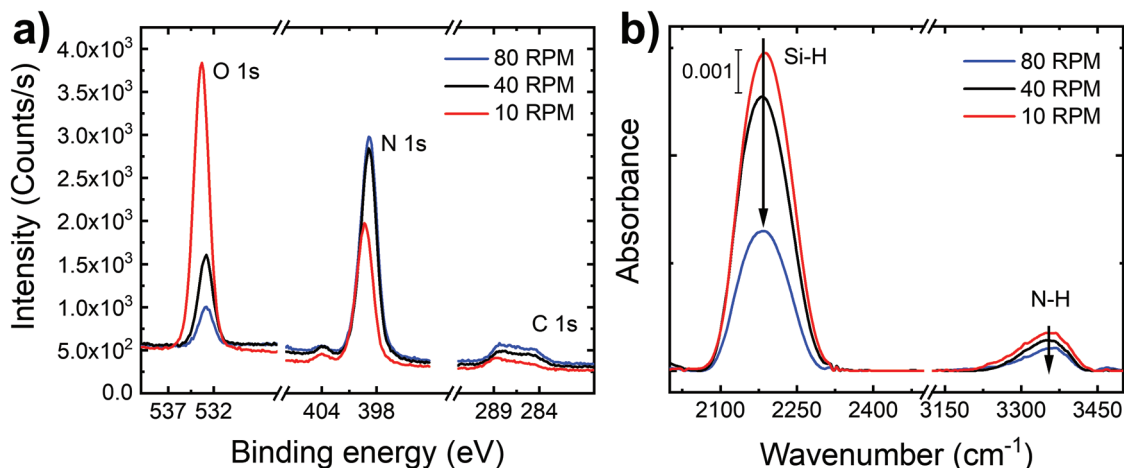
Figure 6. a) Raw XPS data for O1s, N1s and C1s within the bulk part of SiN_x; **b)** baseline-subtracted Si-H and N-H modes as measured by FTIR. All SiN_x layers were deposited at 200 °C by atmospheric-pressure spatial ALD at 10 RPM (red line), 40 RPM (black line), and 80 RPM (blue line).

By comparing the results obtained in this work with those reported in literature a few conclusions can be drawn. With atmospheric-pressure spatial ALD one can grow films with oxygen contents comparable to low-pressure temporal ALD. The carbon content is even lower than that reported for films grown from BDEAS and high-frequency Capacitively Coupled N_2 plasma (CCP) in low-pressure temporal PE-ALD,[10] and comparable to the films grown from bis(tert-butyl)aminosilane (BTBAS) in combination with N_2 plasma, yet much higher than those obtained by di(sec-butyl)aminosilane (DSBAS) and TSA in combination with N_2 plasma.

It is likely that the oxygen contaminations in the case of spatial ALD are originated by O_2 and H_2O traces that are present in the background ambient of the reactor, similarly to what reported for the atmospheric pressure PE-CVD process using $SiH_4/N_2/He$ [12].

Table 1. Short overview of vapor phase deposition of thin SiN_x films. AP = Atmospheric pressure; PE = plasma-enhanced; CVD = Chemical Vapor deposition; ALD = Atomic Layer Deposition; CCP = capacitively coupled plasma; ICP = inductively coupled plasma; d.l. = detection limit; ECR= Electron Cyclotron Resonance.

Deposition method	Precursor(s)	Plasma source	Deposition temperature (°C)	Dep. rate (nm/min)	Growth per cycle (Å)	Refractive index	Composition					Reference
							N/Si	O at.%	C (at.%)	H (at.%)	H- density (cm⁻³)	
PE-CVD	$SiH_4/N_2/He$	CCP RF	250	4.4	n.a.	1.928	1.36	n.a.	n.a.	n.a.	8.4×10^{21}	[25]
	SiH_4/N_2	CCP RF	250	6.5	n.a.	2.348		n.a.	n.a.	n.a.	17.3×10^{21}	[25]
	$SiH_4/NH_3/N_2$	ICP	200	~18	n.a.	1.90	~1.2	n.a.	n.a.	~32	n.a.	[28]
	SiH_4/N_2	ICP	200	~20	n.a.	1.86	~1.3	n.a.	n.a.	~21	n.a.	[28]
	$SiH_4/N_2/N_2$	ECR	250	3	n.a.	1.94	~1.3	n.a.	n.a.	1.5	4.5×10^{21}	[29]
AP-PE-CVD	$SiH_4/N_2/He$	Parallel plate electrodes	200	50	n.a.	n.a.	1.22−1.45	6.3	0.15	32[a]	n.a.	[12]
PE-ALD	TSA/N_2	ICP	240	0.08	1.20	1.94	0.84	6	< d.l.		n.a.	[30]
	$DSBAS/N_2$	ICP	200	0.04	0.12	1.89	1.2	4	4	8	n.a.	[7]
	$BTBAS/N_2$	ICP	200	0.09	0.32	1.83	1.7	5	9	11	n.a.	[7]
	$BDEAS/N_2$	CCP	200	0.3	2.30	n.a.	0.84	15.9	17.9	n.a.	n.a.	[10]
AP-PE-spatial-ALD	$BDEAS/N_2$	DBD	200	1.52	0.19	1.87	1.34	4.7	13.9		35×10^{21}	This work

a = value estimated assuming linear decrease from 37.5 at.% H at 100 °C to 13.9 at. % at 500 °C.

Since carbon incorporation within the bulk of the SiN_x films originates either from incomplete removal of the precursor's ligands or from redeposition effects, one can expect that atmospheric-pressure spatial ALD using precursors with better exchangeable ligand groups such as BTBAS, or carbon-free precursors such as trisilylamine or neopentasilane will result in much lower carbon contaminations thus further improving the SiN_x quality. Alternatively, a dual-plasma approach with an H_2/N_2 plasma exposure followed by an N_2 plasma can be developed in order to drive out even more carbon.

Regarding the hydrogen content, a direct comparison could not be made because of the different measurement methods present in the literature: infrared spectroscopy and elastic recoil detection.

When comparing the different vapor phase deposition methods listed in Table 1, a clear difference can be observed between the deposition rates at atmospheric-pressure and those at low-pressure. For atmospheric pressure PE-CVD much higher deposition rates have been reported compared to low-pressure PE-CVD, likewise atmospheric-pressure spatial ALD can afford between ~8 to 42 times higher deposition rates than temporal ALD, which almost approach the ones obtained by PE-CVD. Finally, it should be noticed that by optimizing the spatial ALD reactor design even higher deposition rates may become accessible.

4. Conclusions

A world-first low-temperature ($\leq$ 250 °C) atmospheric-pressure spatial ALD process for SiN_x has been developed, which can reach comparably low oxygen atomic percentage as those obtained by low-pressure temporal ALD processes based on similar chemistries. At the same time, deposition rates up to 42 times higher than temporal ALD were measured, *i.e.* 1.5 nm/min, thus almost approaching the deposition rates of low-pressure PE-CVD processes.

With the current reactor configuration we show that the N_2 plasma step has a strong impact on the resulting layer composition and that short plasma exposure and cycle times lead to low oxygen contents. We speculate that this may be due to O_2 and H_2O traces being present as impurities in the background ambient and in the N_2 gas lines, or due to plasma-induced outgassing of the ceramic elements of the DBD plasma source. Whilst carbon contamination still remains a concern for the current process, we foresee that different precursor chemistries will lead to improved film composition and that especially N_2 purifiers will allow for obtaining SiN_x compositions that are less dependent on plasma exposure. Such independency will probably be a prerequisite prior to testing the atmospheric-pressure spatial ALD process on high-aspect ratio structures.

We believe that the results presented in this work will enrich the toolbox of spatial ALD processes and open pathways for high-throughput spatial ALD of silicon nitrides, and other relevant nitrides like titanium nitride, at atmospheric pressure, thus making it compatible with sheet-to-sheet, roll-to-roll as well as semi batch-type of reactors for high-throughput atomic-level processing.

Acknowledgments

References

1. A. M. Andringa, A. Perrotta, K. De Peuter, H. C. M. Knoops, W. M. M. Kessels, and M. Creatore, "Low-Temperature Plasma-Assisted Atomic Layer Deposition of Silicon Nitride Moisture Permeation Barrier Layers," *ACS Appl. Mater. Interfaces*, vol. 7, no. 40, pp. 22525–22532, 2015. https://doi.org/10.1021/acsami.5b06801

2. X. Meng, Y. C. Byun, H. S. Kim, J. S. Lee, A. T. Lucero, L. Cheng, and J. Kim, "Atomic Layer Deposition of Silicon Nitride Thin Films: A Review of Recent Progress, Challenges, and Outlooks," *Materials (Basel).*, vol. 9, no. 12, p. 1007, 2016. https://doi.org/10.3390/ma9121007

3. H. S. Kim, X. Meng, S. J. Kim, A. T. Lucero, L. Cheng, Y. C. Byun, J. S. Lee, S. M. Hwang, A. L. N. Kondusamy, R. M. Wallace, G. Goodman, A. S. Wan, M. Telgenhoff, B. K. Hwang, and J. Kim, "Investigation of the Physical Properties of Plasma Enhanced Atomic Layer Deposited Silicon Nitride as Etch Stopper," *ACS Appl. Mater. Interfaces*, vol. 10, no. 51, pp. 44825–44833, 2018. https://doi.org/10.1021/acsami.8b15291

4. M. A. Mione, V. Vandalon, A. Mameli, W. M. M. Kessels, and F. Roozeboom, "Atmospheric-Pressure Plasma-Enhanced Spatial ALD of SiO_2 Studied by Gas-Phase Infrared and Optical Emission Spectroscopy," *J. Phys. Chem. C*, vol. 125, no. 45, pp. 24945–24957, 2021. https://doi.org/10.1021/acs.jpcc.1c07980

5. G. Dingemans, C. A. A. van Helvoirt, M. C. M. van de Sanden, and W. M. M. Kessels, "Plasma-assisted Atomic Layer Deposition of Low Temperature SiO_2," *ECS Trans.*, vol. 35, no. 4, pp. 191–204, 2011. https://doi.org/10.1149/1.3572283

6. R. H. E. C. Bosch, L. E. Cornelissen, H. C. M. Knoops, and W. M. M. Kessels, "Atomic Layer Deposition of Silicon Nitride from Bis(tertiary-butyl-amino)silane and N_2 Plasma Studied by in Situ Gas Phase and Surface Infrared Spectroscopy," *Chem. Mater.*, vol. 28, no. 16, pp. 5864–5871, 2016. https://doi.org/10.1021/acs.chemmater.6b02319

7. T. Faraz, M. van Drunen, H. C. M. Knoops, A. Mallikarjunan, I. Buchanan, D. M. Hausmann, J. Henri, and W. M. M. Kessels,, "Atomic layer deposition of wet-etch resistant silicon nitride using di(*sec*-butylamino)silane and N_2 plasma on planar and 3D Substrate topographies," *ACS Appl. Mater. Interfaces*, vol. 9, no. 2, pp. 1858–1869, 2017. https://doi.org/10.1021/acsami.6b12267

8. H. C. M. Knoops, E. M. J. Braeken, K. de Peuter, S. E. Potts, S. Haukka, V. Pore, and W. M. M. Kessels, "Atomic Layer Deposition of Silicon Nitride from Bis(*tert* - butylamino)silane and N_2 Plasma," 2015. https://doi.org/10.1021/acsami.5b06833

9. S. Weeks, G. Nowling, N. Fuchigami, M. Bowes, and K. Littau, "Plasma enhanced atomic layer deposition of silicon nitride using neopentasilane," *J. Vac. Sci. Technol. A Vacuum, Surfaces, Film.*, vol. 34, no. 1, p. 01A140, 2016. https://doi.org/10.1116/1.4937993

10. J. Y. Byun, Y. J. Ji, K. H. Kim, K. S. Kim, H. W. Tak, A. R. Ellingboe, and G. Y. Yeom, "Characteristics of silicon nitride deposited by very high frequency (162 MHz)-plasma enhanced atomic layer deposition using bis(diethylamino) silane," *Nanotechnology*, vol. 32, no. 7, 2021. https://doi.org/10.1088/1361-6528/abb974

11. H. Kakiuchi, Y. Nakahama, H. Ohmi, K. Yasutake, K. Yoshii, and Y. Mori, "Investigation of deposition characteristics and properties of high-rate deposited silicon nitride films prepared by atmospheric pressure plasma chemical vapor deposition," *Thin Solid Films*, vol. 479, no. 1–2, pp. 17–23, 2005. https://doi.org/10.1016/j.tsf.2004.11.104

12. G. R. Nowling, S. E. Babayan, V. Jankovic, and R. F. Hicks, "Remote plasma-enhanced chemical vapour deposition of silicon nitride at atmospheric pressure," *Plasma Sources Sci. Technol.*, vol. 11, no. 1, pp. 97–103, 2002. https://doi.org/10.1088/0963-0252/11/1/312

13. P. Poodt, D. C. Cameron, E. Dickey, S. M. George, V. Kuznetsov, G. N. Parsons, F. Roozeboom, G. Sundaram, and A. Vermeer, "Spatial atomic layer deposition: A route towards further industrialization of atomic layer deposition," *J. Vac. Sci. Technol. A Vacuum, Surfaces, Film.*, vol. 30, no. 1, p. 010802, 2012. https://doi.org/10.1116/1.3670745

14. A. Mameli, J. D. Parish, T. Dogan, G. Gelinck, M. W. Snook, A. J. Straiton, A. L. Johnson, and A. J. Kronemeijer, "High-Throughput Atomic Layer Deposition of P-Type SnO Thin Film Transistors Using Tin(II)bis(*tert*-amyloxide)," *Adv. Mater. Interfaces*, vol. 9, no. 9, pp. 1–8, 2022. https://doi.org/10.1002/admi.202101278

15. M. A. Mione, R. Engeln, V. Vandalon, W. M. M. Kessels, and F. Roozeboom, "Infrared and optical emission spectroscopy study of atmospheric pressure plasma-enhanced spatial ALD of Al_2O_3," *Appl. Phys. Lett.*, vol. 115, no. 8, 2019. https://doi.org/10.1063/1.5113753

16. D. Muñoz-Rojas, V. H. Nguyen, C. Masse de la Huerta, S. Aghazadehchors, C. Jiménez, and D. Bellet, "Spatial Atomic Layer Deposition (SALD), an emerging tool for energy materials. Application to new-generation photovoltaic devices and transparent conductive materials," *Comptes Rendus Phys.*, vol. 18, no. 7–8, pp. 391–400, 2017. https://doi.org/10.1016/j.crhy.2017.09.004

17. C. A. M. de la Huerta, V. H. Nguyen, A. Sekkat, C. Crivello, F. Toldra-Reig, P. B. Veiga, S. Quessada, C. Jimenez, and D. Muñoz-Rojas, "Gas-Phase 3D Printing of Functional Materials," *Adv. Mater. Technol.*, vol. 5, no. 12, pp. 1–8, 2020. https://doi.org/10.1002/admt.202000657

18. N. Boysen, B. Misimi, A. Muriqi, J. L. Wree, T. Hasselmann, D. Rogalla, T. Haeger, D. Theirich, M. Nolan, T. Riedl, and A. Devi, "A carbene stabilized precursor for the spatial atomic layer deposition of copper thin films," *Chem. Commun.*, vol. 56, no. 89, pp. 13752–13755, 2020. https://doi.org/10.1039/D0CC05781A

19. F. J. van den Bruele, M. Smets, A. Illiberi, Y. Creyghton, P. Buskens, F. Roozeboom, and P. Poodt, "Atmospheric pressure plasma enhanced spatial ALD of silver," *J. Vac. Sci. Technol. A Vacuum, Surfaces, Film.*, vol. 33, no. 1, p. 01A131, 2015. https://doi.org/10.1116/1.4902561

20. A. Illiberi, R. Scherpenborg, F. Roozeboom, and P. Poodt, "Atmospheric Spatial Atomic Layer Deposition of In-Doped ZnO," *ECS J. Solid State Sci. Technol.*, vol. 3, no. 5, pp. P111–P114, 2014. https://doi.org/10.1149/2.002405jss

21. Y. Creyghton, A. Illiberi, M. Mione, W. van Boekel, N. Debernardi, M. Seitz, F. Bruele, P. Poodt, and F. Roozeboom, "Developments in Plasma-Enhanced Spatial ALD for High-Throughput Applications," in *Proc. Int. Conf. on Coatings on Glass and Plastics (ICCG 2016)*, 2016, pp. 93–97.

22. M. A. Mione, I. Katsouras, Y. Creyghton, W. van Boekel, J. Maas, G. Gelinck, F. Roozeboom, and A. Illiberi, " Atmospheric Pressure Plasma Enhanced Spatial ALD of ZrO_2 for Low-Temperature, Large-Area Applications ," *ECS J. Solid State Sci. Technol.*, vol. 6, no. 12, pp. N243–N249, 2017. https://doi.org/10.1149/2.0381712jss

23. A. Illiberi, I. Katsouras, S. Gazibegovic, B. Cobb, E. Nekovic, W. van Boekel, C. Frijters, J. Maas, F. Roozeboom, Y. Creyghton, P. Poodt, and G. Gelinck, "Atmospheric plasma-enhanced spatial-ALD of InZnO for high mobility thin film transistors," *J. Vac. Sci. Technol. A Vacuum, Surfaces, Film.*, vol. 36, no. 4, p. 04F401, 2018. https://doi.org/10.1116/1.5008464

24. W. A. Lanford and M. J. Rand, "The hydrogen content of plasma-deposited silicon nitride," *J. Appl. Phys.*, vol. 49, no. 4, pp. 2473–2477, 1978. https://doi.org/10.1063/1.325095

25. G. N. Parsons, J. H. Souk, and J. Batey, "Low hydrogen content stoichiometric silicon nitride films deposited by plasma-enhanced chemical vapor deposition," *J. Appl. Phys.*, vol. 70, no. 3, pp. 1553–1560, 1991. https://doi.org/10.1063/1.349544

26. H. C. M. Knoops, K. De Peuter, and W. M. M. Kessels, "Redeposition in plasma-assisted atomic layer deposition : Silicon nitride film quality Redeposition in plasma-assisted atomic layer deposition : Silicon nitride film quality ruled by the gas residence time," vol. 014102, 2015. https://doi.org/10.1063/1.4926366

27. C. K. Ande, H. C. M. Knoops, K. de Peuter, M. van Drunen, S. D. Elliott, and W. M. M. Kessels, "Role of Surface Termination in Atomic Layer Deposition of Silicon Nitride," *J. Phys. Chem. Lett.*, vol. 6, no. 18, pp. 3610–3614, 2015. https://doi.org/10.1021/acs.jpclett.5b01596

28. F. Karouta, K. Vora, J. Tian, and C. Jagadish, "Structural, compositional and optical properties of PECVD silicon nitride layers," *J. Phys. D. Appl. Phys.*, vol. 45, no. 44, 2012. https://doi.org/10.1088/0022-3727/45/44/445301

29. J. R. Flemish and R. L. Pfeffer, "Low hydrogen content silicon nitride films from electron cyclotron resonance plasmas," *J. Appl. Phys.*, vol. 74, no. 5, pp. 3277–3281, 1993. https://doi.org/10.1063/1.355318

30. H. S. Kim , S. M. Hwang, X. Meng, Y. C. Byun, Y. C. Jung, A. V. Ravichandran, A.Sahota, S. J. Kim, J. Ahn, L. Lee, X. Zhou, B. K. Hwang, and J. Kim, "High growth rate and high wet etch resistance silicon nitride grown by low temperature plasma enhanced atomic layer deposition with a novel silylamine precursor," *J. Mater. Chem. C*, vol. 8, no. 37, pp. 13033–13039, 2020. https://doi.org/10.1039/D0TC02866E

E-mail and ORCID

Jie Shen (jie.shen@tno.nl), ⓘ ORCID: https://orcid.org/0009-0001-8331-2610
Fred Roozeboom (f.roozeboom@utwente.nl), ⓘ ORCID: https://orcid.org/0000-0003-3925-7041
Alfredo Mameli (Corresponding author, alfredo.mameli@tno.nl), ⓘ ORCID: https://orcid.org/000-0001-9175-8965

Supplementary material 1

Supplementary table and figures

Authors: Jie Shen, Fred Roozeboom, Alfredo Mameli

Data type: figures and table (docx file)

Explanation note: table S1. Material properties as a function of the rotation speed, at a deposition temperature of 200 °C. figure S1. Growth per cycle for atmospheric pressure spatial ALD of SiNx at a rotation speed of 20 RPM and a deposition temperature of 250 °C. figure S2. XPS depth-profiles for SiNx layers deposited by atmospheric pressure spatial ALD at 200 °C and rotation speed of: a) 80 RPM; b) 40 RPM; c) 10 RPM

Link: https://doi.org/10.3897/aldj.1.101651.suppl1